

# Characterization of silver selenide thin films grown on Cr-covered Si substrates

Bhaskar Chandra Mohanty,<sup>a,†</sup> P. Malar,<sup>b</sup> Thomas Osipowicz,<sup>b</sup> B. S. Murty,<sup>c</sup> Shikha Varma<sup>d</sup> and S. Kasiviswanathan<sup>a\*</sup>

**Thermal stability of silver selenide thin films formed from the solid-state reaction of Ag-Se diffusion couples on Si substrates covered with a thin Cr film, is investigated. Glancing angle X-ray diffraction (GXR), XPS, atomic force microscopy (AFM) and Rutherford backscattering spectrometry (RBS) are used to characterize the as-deposited films and those annealed at 100, 200, 300, and 400 °C. The results reveal the formation of polycrystalline orthorhombic silver selenide films that remain stable without compositional change upon thermal annealing, in marked contrast to the agglomeration exhibited by silver selenide films deposited on Si without Cr film. The improvement in the thermal stability is attributed to compressive stress relief by a grainy morphology with large surface area, the formation of which is promoted by partially oxidized Cr adhesion film. Copyright © 2008 John Wiley & Sons, Ltd.**

**Keywords:** Ag<sub>2</sub>Se; AFM; XPS; RBS; thermal stability

## Introduction

One of the key roles played by buffer layers in thin film technology is in improving the thermal stability<sup>[1]</sup> of films which can otherwise become unstable. For instance, high temperature process conditions can lead to thin film agglomeration which adversely affects the device performance and, consequently, device reliability. Insertion of a buffer layer or combination of such layers between a thin film and substrate creates new interfaces replacing the original one, but enhances adhesion and thereby the thermal stability of the film. Buffer layers, apart from providing stability at elevated temperature, can promote textured growth of the overlayer films or act as barrier layers against diffusion/electromigration as well.<sup>[2,3]</sup>

The choice of a specific buffer layer is principally determined by the nature of the problem that needs to be circumvented. In Cu metallization, Cu readily diffuses into Si and, in addition, exhibits poor adhesion to dielectric substrates. This problem is overcome by interposing thin films of refractory metals/metal nitrides or a bilayer such as TaN-Ta.<sup>[3]</sup> Detailed studies on the textured growth of noble metal films have shown the existence of a strong relationship between texturing and the underlying buffer layer. For instance, Ti underlayer greatly improves the thermal stability of Ag films on oxide substrates and simultaneously aids the textured (111) growth of Ag.<sup>[4]</sup> Buffer layers can also help improve certain physical and chemical properties of overlayer films. For example, a Cu underlayer has been shown to reduce the ordering temperature as well as to enhance the formation of L<sub>10</sub>-CoPt phase,<sup>[5]</sup> whereas a Ta adhesion layer is found to improve the ferroelectric properties of SrBi<sub>2</sub>Ta<sub>2</sub>O<sub>9</sub> thin films considerably.<sup>[6]</sup>

In this communication, we report the results of our investigation on the effect of a thin Cr film on the thermal stability of silver selenide films formed from the solid-state reaction of Ag and Se on Si substrates. Silver selenide, one of the well-known metal chalcogenides, has been widely studied for its polymorphic phase transition, high ionic conductivity, and large thermoelectric

power.<sup>[7]</sup> It has attracted much attention after the discovery of huge magneto resistance, the origin of which has been attributed to the presence of nanoscale metal clusters in an otherwise semiconducting matrix.<sup>[8]</sup> Recently, we have studied the thermal stability of silver selenide films grown on Si from the room temperature reaction of Ag-Se diffusion couples.<sup>[9,10]</sup> When the films are subjected to heat treatment, the morphology of the films becomes unstable and eventually the films agglomerate completely into islands at 400 °C.<sup>[9,10]</sup> We have examined whether a thin Cr buffer layer can improve the stability of the silver selenide films on Si. Cr has been chosen as the adhesion promoter since it has been widely used to improve the adhesion of noble metal films to different substrates. In the present work, inhibition of agglomeration of silver selenide films on Si promoted by Cr buffer layer is elucidated in terms of the morphological evolution and relief of stress. The phase of the films is identified from the analysis of Glancing angle X-ray diffraction (GXR) patterns. Analysis of Ag 3d and Se 3d core level spectra obtained from XPS measurements show that there are no noticeable changes in their binding energies with anneal temperature, indicative of unperturbed Ag-Se bonds. A detailed analysis of surface morphology of the

\* Correspondence to: Dr. S. Kasiviswanathan, Department of Physics, Indian Institute of Technology Madras, Chennai, 600 036, India. E-mail: kasi@iitm.ac.in

† Present address: Department of Materials Science and Engineering, Yonsei University, 134 Sinchon-dong, Seodaemun-gu, Seoul 120-749, Korea.

a Department of Physics, Indian Institute of Technology Madras, Chennai, 600 036, India

b Department of Physics, Centre for Ion Beam Applications, National University of Singapore, 119260, Singapore

c Department of Metallurgical and Materials Engineering, Indian Institute of Technology Madras, Chennai, 600 036, India

d Institute of Physics, Bhubaneswar 751005, India

films as a function of annealing temperature is carried out using atomic force microscopy (AFM). The compositions of elements in a particular layer and the interlayer integrity have been investigated using Rutherford backscattering spectrometry (RBS). The results show that thin Cr film, though partially oxidized, greatly improves the thermal stability of silver selenide films.

## Experimental Details

Silver selenide films used in this study were grown by the solid-state reaction of sequentially deposited Se and Ag films.<sup>[9]</sup> Initially, a thin Cr film was deposited onto Si (100) substrates that were subjected to 10% HF etch for about 30 s before being taken into the Cr metallization chamber. The substrates were then exposed to Ar (99.9%) glow discharge for about 20 min at a chamber pressure of  $\sim 0.1$  mbar prior to the deposition of Cr. After the Cr deposition, vacuum was broken by introducing Ar gas and the Cr/Si samples were transferred to another chamber for the growth of silver selenide thin films. In order to remove any adsorbed water vapor, the Cr/Si samples were exposed to Ar glow discharge under similar conditions mentioned earlier. Silver selenide films were formed by first depositing Se film followed by the deposition of Ag film of suitable thickness. The time interval between the deposition of Cr and Se films was about 4 h. All the films were grown at a pressure level of  $\sim 2 \times 10^{-6}$  mbar. During the film growth, the substrates were held at room temperature ( $\sim 27^\circ\text{C}$ ). The rate of deposition and film thickness were monitored by a quartz crystal thickness monitor. The Ag and Se films were deposited at a rate of  $\sim 10 \text{ \AA s}^{-1}$  while the Cr film was grown at a rate of  $\sim 0.1 \text{ \AA s}^{-1}$ . The thickness of the silver selenide film was about 160 nm and the Cr film thickness was in the range of 5–12 nm. Silver selenide has an extremely narrow phase field<sup>[8,11]</sup> and hence it is important to discuss the error involved in the ratio of silver and selenium concentrations. The accuracies in the film thickness and rate of evaporation measurements are 0.1 and  $0.01 \text{ nms}^{-1}$ , respectively. This leads to an error ( $\Delta\delta$ ) of  $2 \times 10^{-3}$ , where  $\delta$  is the deviation in the concentration of silver from its ideal value of 2, in silver selenide ( $\text{Ag}_{2\pm\delta}\text{Se}$ ).

The as-deposited films were annealed at 100, 200, 300, and  $400^\circ\text{C}$  for 60 min in flowing pure (99.9%) argon. Annealing was carried out in a tubular furnace, the temperature of which was controlled to an accuracy of  $\pm 1^\circ\text{C}$ . The phase of the as-deposited films was identified from the GXR D studies. Since the penetration depth of X-rays can be controlled by the incident angle, it is possible to get surface-specific information using GXR D. The GXR D measurements were made using a PANalytical model X'Pert PRO XRD unit using  $\text{Cu-K}\alpha$  radiation at four different glancing angles, viz.  $0.33^\circ$ ,  $0.50^\circ$ ,  $0.80^\circ$  and  $1.00^\circ$  and at steps of  $0.04^\circ$  in  $2\theta$  values. The photoelectron spectra were obtained with a ESCA-2000 Multilab apparatus (VG Microtech) using a nonmonochromatic  $\text{Mg K}\alpha$  excitation source and a hemispherical analyzer. The residual gas pressure in the chamber during the measurements was  $\sim 10^{-10}$  Torr. All spectra were recorded at  $90^\circ$  take-off angle with a pass energy of 20 eV and at an instrumental resolution of 0.9 eV. After obtaining a survey scan in the energy range 0–1000 eV, core spectra of elements, namely Ag 3d, Se 3d and C 1s were recorded for all the films. The binding energies were corrected with reference to the C 1s line at 284.6 eV. RBS experiments were performed using normally incident  $^4\text{He}^+$  beam having energy of 2 MeV and with a beam current in the order of 5 nA. The scattered particles were collected through a surface barrier detector positioned at an angle of  $160^\circ$ . The backscattering

spectra were simulated with the help of the software 'SIMNRA'.<sup>[12]</sup> AFM experiments in contact mode were carried out under ambient conditions using Digital Instruments Nanoscope IV SPM system with a silicon nitride cantilever.

## Results and Discussion

### X-ray diffraction

Typical GXR D patterns recorded at glancing angles of  $0.33^\circ$ ,  $0.50^\circ$ ,  $0.80^\circ$  and  $1.00^\circ$  are shown in Figs. 1(a)–(d). The diffraction patterns were recorded after suitably rotating the sample about its normal so that contributions from a maximum number of planes were obtained. The diffraction patterns obtained at incident angles of  $0.33^\circ$  and  $0.50^\circ$  (Fig. 1(a) and (b)) are similar in nature. The patterns contain several sharp peaks, all of which could be identified with those arising from the various planes of  $\text{Ag}_2\text{Se}$  with orthorhombic phase.<sup>[13]</sup> The relative intensities of the peaks, however, differed considerably from the standard data. This may be because the planes that have contributed to the diffraction intensity may not be as randomly oriented as in a bulk powdered sample.

The diffraction patterns recorded at angles of incidences of  $0.80^\circ$  and  $1.00^\circ$  (Fig. 1(c) and (d)) appear similar to those measured at  $0.33^\circ$  and  $0.50^\circ$ , but for the presence of two additional peaks (marked by arrows, in Fig. 1(c)) at  $52.18^\circ$  and  $54.14^\circ$ . In GXR D, as the angle of incidence is increased, the diffraction pattern will contain contributions from buried regions as well. It is important to note here that these peaks, however, are not present in XRD patterns recorded using conventional geometry used for bulk specimens. In fact, we have carried out detailed XRD measurements using conventional geometry of the as-deposited film and those annealed at 100, 200, 300, and  $400^\circ\text{C}$ . The films annealed at  $200^\circ\text{C}$  show a strong preferential orientation along the (200) plane which changes to (013) after annealing at  $300^\circ\text{C}$  and continues to show (013) orientation even after annealing at  $400^\circ\text{C}$ . The XRD results along with dynamic secondary ion mass spectrometry

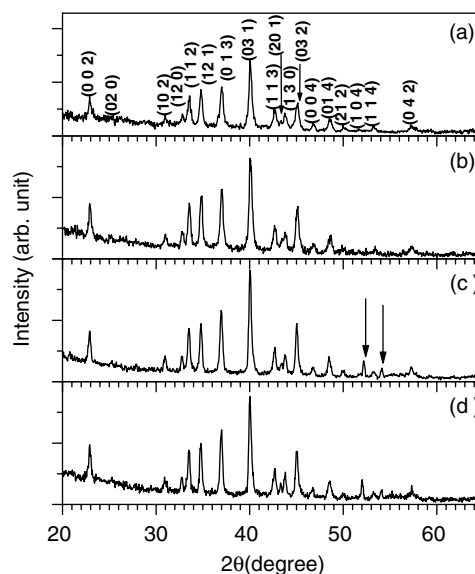


**Figure 1.** Typical GXR D pattern of silver selenide thin films at glancing angle (a)  $0.33^\circ$ , (b)  $0.50^\circ$ , (c)  $0.80^\circ$ , and (d)  $1^\circ$ . The films were grown from room temperature reaction of Ag/Se bilayers on  $\sim 10$  nm thick Cr film-covered Si substrates.

studies are presented elsewhere.<sup>[14]</sup> The fact that these additional peaks appear in GXR patterns recorded at angles  $0.80^\circ$  and  $1.00^\circ$  and they are not observed in XRD data obtained in bulk mode shows that they arise from a thin subsurface region below the silver selenide film. The angles at which they appear coincide with those expected for  $\text{SiO}_2$ .<sup>[15]</sup> However, they cannot be attributed to  $\text{SiO}_2$  as the native oxide, if any, formed under the present process conditions must be amorphous in nature. The other possible sources are regions with elemental Cr or suboxides of Cr or a composite region comprising of Cr, O, and Si. Cr does not have a diffraction signal at these angles, although a small shoulder to signal from 014 plane (visible on an expanded scale) that may be attributed to (211) plane of elemental Cr is present. However, Cr has several oxidation states and we believe that the peaks may be due to suboxides of Cr. In fact, our RBS results do show evidence for this presumption and the details are presented in the subsequent sections.

### AFM studies

Typical AFM images showing the evolution of surface morphology of silver selenide films with increase in annealing temperature are presented in Fig. 2. All the images have the same scan

area of  $5\ \mu\text{m} \times 5\ \mu\text{m}$ . The as-deposited film (Fig. 2(a)) shows the formation of well-developed grains. Besides, it shows the growth of randomly distributed grain clusters which may have formed from the aggregation of smaller grains. One such grain cluster is marked by an arrow in Fig. 2(a). The average grain size and the rms roughness of the film are found to be about 90 and 20 nm respectively. A careful examination of the image shows that there is a nonuniform distribution of grains. The image (Fig. 2(a)) contains regions dominated by densely packed grains (nearly at the middle) as well as areas (top of the image, for example) which have isolated dark spots and multiple dark spots that are connected to each other. These dark spots may represent missing grains since a film, depending on its thickness, may contain several grains across its height. Alternatively, they may be physical holes extending down to the substrate. Given the film thickness of  $\sim 160$  nm and the well-developed spherically shaped grains with an average size of  $\sim 90$  nm, possibly, the dark spots are physical holes. In such cases, the interconnected dark spots may represent cracks in the film. When the film is annealed at  $100^\circ\text{C}$  (Fig. 2(b)), there is an appreciable increase in the average grain size ( $\sim 150$  nm) without visible change in grain shape, and the rms roughness increased to  $\sim 24$  nm. Annealing at  $200^\circ\text{C}$  (Fig. 2(c)) resulted in a

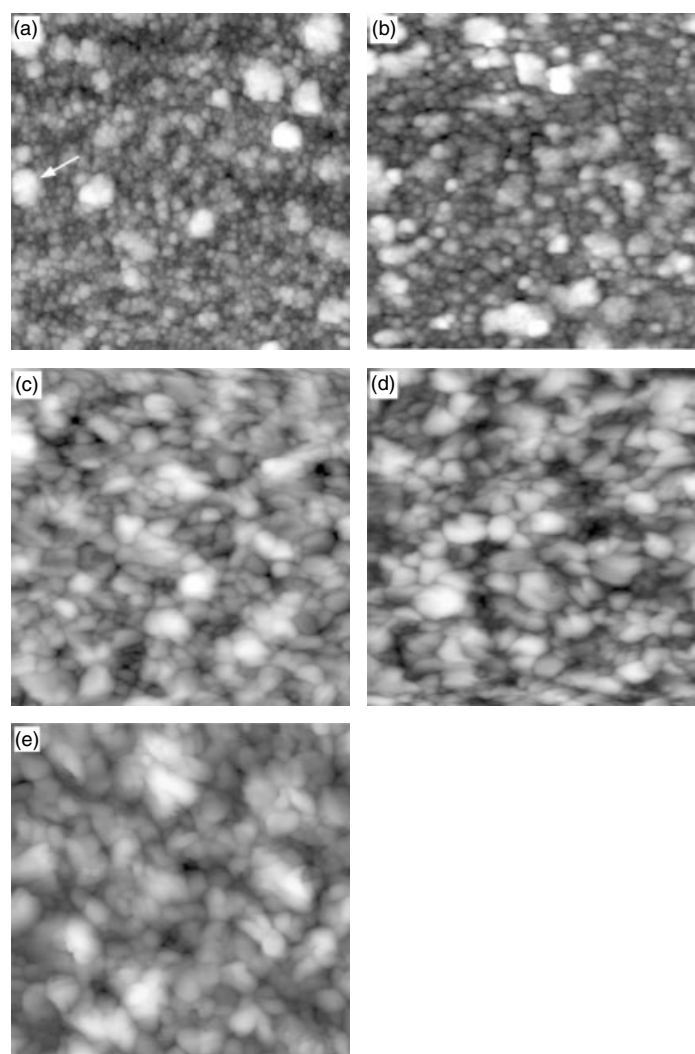


**Figure 2.** Representative AFM images ( $5\ \mu\text{m} \times 5\ \mu\text{m}$  scanned area) of (a) as-deposited film and films annealed at (b) 100, (c) 200, (d) 300, and (e)  $400^\circ\text{C}$  respectively. The arrow in (a) indicates a grain cluster.

marked change in the grain shape as well as a large distribution in the size. Further, the size of the holes increased and the holes appeared mainly near the grain boundaries. The observed uneven changes in the grain shape and size may have been caused by the combined effects of growth of smaller grains and the coalescence of grains in the grain clusters into single larger grains. Analysis of the image yielded an average grain size of  $\sim 230$  nm and an rms roughness of  $\sim 22$  nm. Annealing at  $300^\circ\text{C}$  (Fig. 2(d)) has not resulted in significant change in grain shape, but the average grain size increased to  $\sim 275$  nm while the rms roughness decreased to  $\sim 20$  nm. The holes are still present in the film, but there is a reduction in their number density. The film annealed at  $400^\circ\text{C}$  is free of grain clusters and shows a dense packing of grains (average size  $\sim 290$  nm and film rms roughness  $\sim 18$  nm) which are almost uniform in size and shape. In addition, there is a large reduction in the number density of holes indicating that there is considerable redistribution of material. It may be concluded from the results of thermal annealing that average grain size displays an initial marked increase, followed by a tendency to saturate as the anneal temperature is raised to  $400^\circ\text{C}$ . On the other hand, the rms surface roughness exhibits a marginal rise followed by a gradual decrease. The holes show a considerable increase in their size, but their number density decreases significantly as the anneal temperature is increased. The observed trend in the evolution of the surface morphology reflects the excellent thermal stability of silver selenide films grown on thin Cr-covered Si. These results are in sharp contrast to the dewetting and agglomeration behavior exhibited by silver selenide films grown on Si without Cr film.<sup>[9,10]</sup>

### XPS measurements

The XPS survey spectra of the films in the energy range of 0–1000 eV are shown in Fig. 3. The curves a–e in Fig. 3 correspond, respectively to the as-deposited film and those annealed at 100, 200, 300, and  $400^\circ\text{C}$ . The presence of C and O peaks are attributed to the atmospheric exposure of the films. The precise binding energy of a particular element was obtained by repeated scanning over a narrow energy range, identified from the survey scans. The Ag and Se XPS spectra were deconvoluted using Gaussian–Lorentzian sum function  $f(E)$  after Shirley background subtraction. The function  $f(E)$  is given as<sup>[16]</sup>

$$f(E) = h(1 - m) \exp\left(-\ln 2 \cdot \left[\frac{2(x - E)}{w}\right]^2\right) + \frac{hm}{1 + \left[\frac{2(x - E)}{w}\right]^2} + hT_s \left[1 - \exp\left(-\ln 2 \cdot \left[\frac{2(x - E)}{w}\right]^2\right)\right] \times \exp\left(-\frac{6.9}{T_L} \left[\frac{2(x - E)}{w}\right]^2\right) \quad (1)$$

where,  $w$  is the width of the peak; the product  $h \cdot w$  shows the area under the peak,  $m$  signifies the amount of mixture of Gaussian and Lorentzian function ( $m = 0$  for 100% Gaussian while for 100% Lorentzian,  $m = 1$ ) and  $E$  is the peak position. The last term on right hand side accounts for the asymmetric tail of the peaks ( $T_s = 0$  for symmetric Gaussian–Lorentzian function). The curves were iteratively fitted for minimum in  $\chi^2$  values. The software XPSPEAK

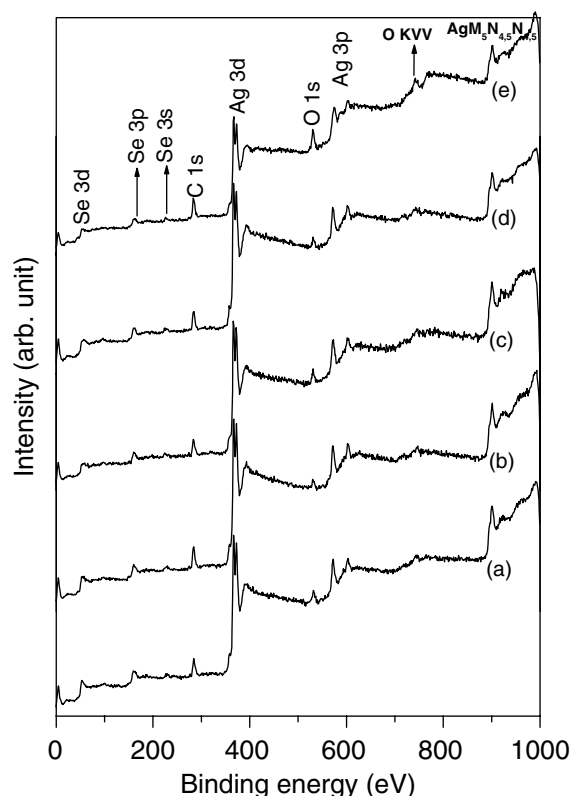


**Figure 3.** XPS survey scans of the silver selenide films on Si with a Cr adhesion layer for (a) as-deposited film and films annealed at (b) 100 (c) 200, (d) 300, and (e)  $400^\circ\text{C}$  for 60 min. in flowing Ar. Measurements were made with Mg- $K_{\alpha}$  X-ray source.

(version 4.1) was used for this purpose. For brevity, the results for the two extreme cases (as-deposited and the films annealed at highest temperature,  $400^\circ\text{C}$ ) alone are discussed in detail and are presented in the following.

Ag 3d XPS spectra in the binding energy range of 362–378 eV for the as-deposited and films annealed at 100, 200, 300, and  $400^\circ\text{C}$  (curves a–e, in that order) are shown in Fig. 4. The spectra consist of two isolated peaks at about 367.8 and 373.8 eV which correspond to the intense spin-orbit doublet of Ag 3d ( $\text{Ag } 3d_{5/2}$  and  $\text{Ag } 3d_{3/2}$ ) from  $\text{Ag}_2\text{Se}$  with spin-orbit splitting of 6.0 eV.<sup>[17]</sup> Two weaker satellite peaks arising owing to the nonmonochromatic nature of the X-ray source are also seen and are marked by arrows in Fig. 4. The differences between the positions of the  $\text{Ag } 3d_{3/2}$  peak and these peaks are 8.4 and 10.3 eV respectively, which correspond to the energy separation between  $K\alpha_3$  and  $K\alpha_4$  from  $K\alpha_{1,2}$  in Mg source.<sup>[18]</sup>

The high resolution experimental (open circles) and fitted (solid line)  $\text{Ag } 3d_{5/2}$  spectra for an as-deposited film and a film annealed at  $400^\circ\text{C}$  are shown in Fig. 5(a) and (b) respectively. The results inferred from the fittings are listed in Table 1. The table also contains data of Se spectra, a discussion of which will appear later. The obtained binding energy values of Ag peaks for the as-deposited film match well with those reported for Ag in  $\text{Ag}_2\text{Se}$ .<sup>[17]</sup> Further, the binding energy and FWHM values of  $\text{Ag } 3d_{5/2}$  peak of the film annealed at  $400^\circ\text{C}$  do not differ noticeably from those observed for the as-deposited film, which shows that the chemical environment of Ag is not altered by the thermal treatment.

Further information about the chemical bonding between Ag and Se was obtained from the investigation of Se 3d photoemission spectra which is shown in Fig. 6. The curves a–e in Fig. 6 corre-

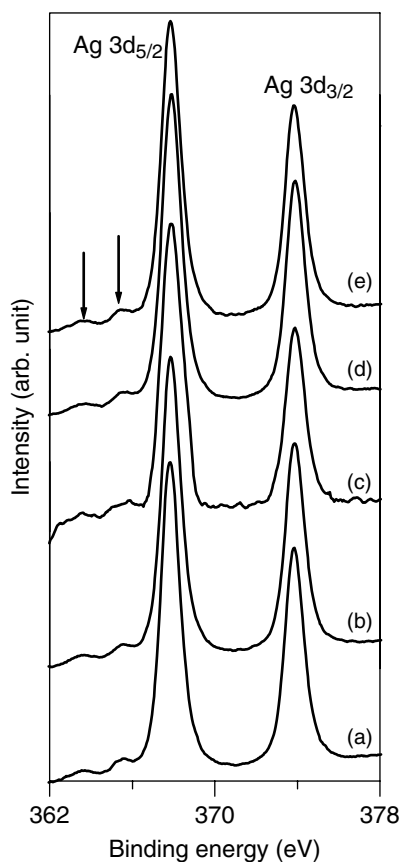


**Figure 4.** Ag 3d photoelectron spectra for silver selenide films: (a) as-deposited film and films annealed at (b) 100 (c) 200, (d) 300, and (e) 400 °C. The arrows indicate the satellite peaks due to nonmonochromatic X-ray source.

**Table 1.** XPS data obtained from the fitting of Ag 3d<sub>5/2</sub> and Se 3d spectra of as-deposited and 400 °C annealed films. The binding energy values were referenced to C 1 s at 284.6 eV

Photoemission line	Peak	Binding energy, eV (FWHM, eV)	
		As-deposited film	Film annealed at 400 °C
Ag 3d <sub>5/2</sub>	1 <sup>a</sup>	367.8 (1.05)	367.8 (1.07)
Se 3d	1 (3d <sub>5/2</sub> )	53.3 (1.04)	53.3 (0.98)
	2 (3d <sub>3/2</sub> )	54.2 (1.02)	54.2 (1.04)

<sup>a</sup> With  $m = 0.1$  and asymmetry parameters  $T_S = 0.15$ ,  $T_L = 42$ ; refer to Eqn (1) in text.

spond to the as-deposited and the films annealed at 100, 200, 300, and 400 °C in that order. The spectra are broad and show a shoulder at ~54.2 eV which suggests overlapping of components. In order to find out the precise positions, the spectra were fitted with a double-Gaussian-peak line function  $f(E) = f_1(E) + f_2(E)$ . Here,  $f_1(E)$  and  $f_2(E)$  have line shapes as defined in equation (1) with  $m = 0$  and  $T_S = 0$ . Figure 7 presents the experimental (open circles) and the fitted (solid lines) curves for Se 3d lines for the as-deposited (curve a) and 400 °C annealed (curve b) films. The parameters obtained from the best fit to the experimental data are given in Table 1. The fittings yielded peaks with a spin-orbit splitting of 0.9 eV. It is observed that the peak positions for the annealed film

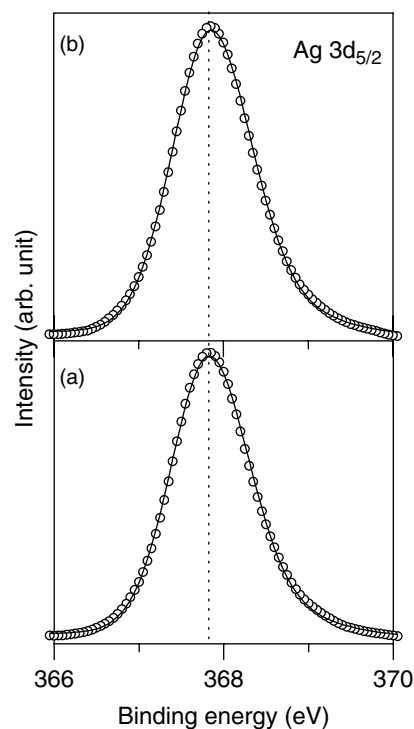


**Figure 5.** Experimental (open circles) and fitted (continuous line) Ag 3d<sub>5/2</sub> spectra of silver selenide thin film: (a) as-deposited and (b) film annealed at 400 °C.

do not differ from those of the as-deposited film, and the binding energy values agree with the reported values of Se in Ag<sub>2</sub>Se.<sup>[19]</sup> While analyzing the data, the presence of additional peaks due to other Se compounds, like selenium oxide, were also searched in this region. The peak corresponding to Se 3d from SeO<sub>2</sub> is expected to occur at ~59.9 eV.<sup>[20]</sup> However, in the Se 3d spectra, there is no peak distinguishable from the background at that energy value, which indicates the absence of SeO<sub>2</sub> on the sample surface.

### RBS analysis

RBS was used to determine the composition of elements in a particular layer and interlayer integrity. RBS analysis was carried out by simulating the experimental data set iteratively and the goodness of the simulations is decided by a  $\chi^2$  minimum test. For brevity, the discussions are limited to two extreme cases: as-deposited films and those annealed at 400 °C, which is the maximum anneal temperature.

Figure 8(a) presents a typical backscattering spectrum (open circles) for the as-deposited sample collected at a scattering angle of 160°. The initial sample configuration considered was a two-layer structure (homogeneous silver selenide film plus Cr film) over a thick Si substrate. A satisfactory simulation of the experimental data, however, required the inclusion of a native oxide layer over Si and also necessitated the incorporation of oxygen in the Cr film. The final sample configuration as determined by the simulations is shown as inset to Fig. 8(a). The best simulation (continuous line) of the experimental data yielded the ratio of the Ag to Se in the top layer to be  $2.00 \pm 0.06$ , and did not require the inclusion of elements, other than Ag and Se. The formation of silver selenide from the solid-state reaction of Ag and Se at room temperature is expected because it is a thermodynamically favorable reaction having a negative free energy of formation of  $-49.4 \text{ kJ mol}^{-1}$ .<sup>[21]</sup>

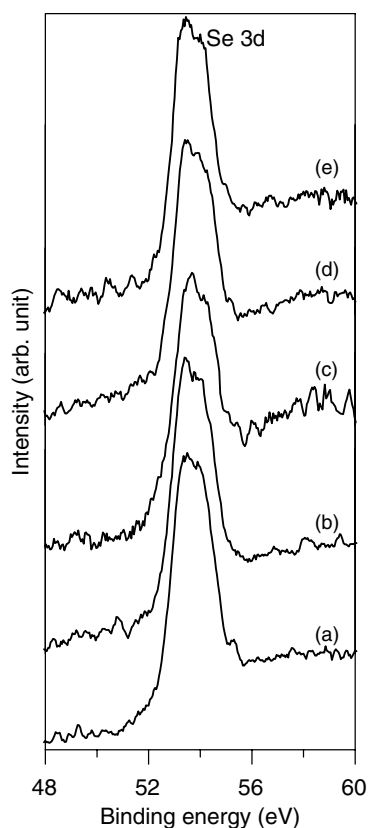


**Figure 6.** Se 3d photoelectron spectra of silver selenide film: (a) as-deposited film and films annealed at (b) 100 (c) 200, (d) 300, and (e) 400 °C.

The immediate underlayer to the top silver selenide film was found to consist of Cr and O with concentrations 83.45 and 16.55% respectively. This inhomogeneous composition of Cr and O indicates the presence of elemental Cr and suboxides of Cr in the layer. The third layer, assumed to be formed directly over the Si substrate, is found to have a composition close to that of SiO<sub>2</sub>, as the simulations yielded the atomic percentage of Si and O, respectively to be 33.34 and 66.66, with a ratio close to 1 : 2.

The backscattering spectra (open circles) recorded for the film annealed at 400 °C are shown in Fig. 8(b). The best simulation (continuous line) of the experimental data revealed the composition of the top layer to be the same as that of the as-deposited sample

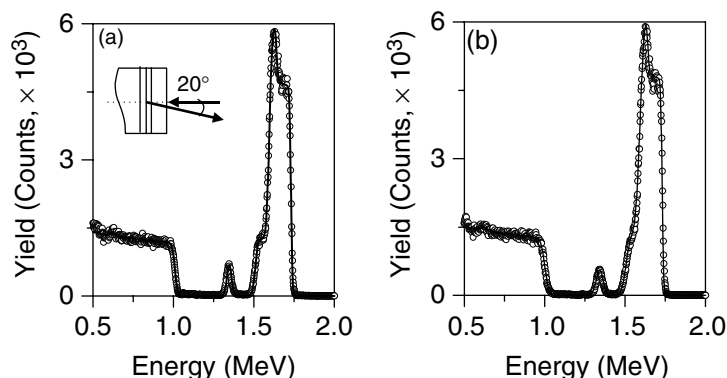


**Figure 8.** Experimental (open circles) and simulated (solid lines) backscattering spectra of (a) as-deposited film and (b) the film annealed at 400 °C. Inset to (a) is the schematic of sample configuration revealed by the simulations.

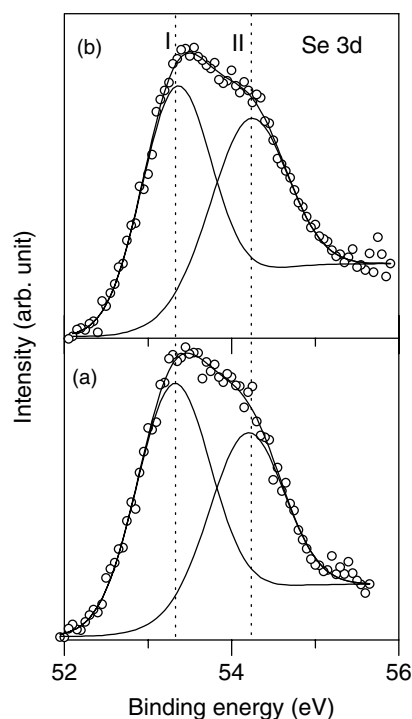


**Figure 7.** Experimental (open circles) and fitted (continuous line) Se 3d spectra of silver selenide thin film: (a) as-deposited and (b) film annealed at 400 °C. The spin-orbit split peaks are marked as I and II.

within experimental uncertainty. The sample configuration obtained from the analysis is the same as that of the as-deposited film. However, the roughness with standard deviation  $\sigma = 13$  nm in the as-deposited film increased to 22 nm. The simulations also revealed a change in composition and the thickness of the second layer. The percentage content of O was found to increase from 16.55 to 31.40%, which shows that the Cr film has been oxidized during annealing. A likely source of oxygen is, presumably, the residual oxygen present in Ar that may have diffused through the holes present in the silver selenide film to reach the Cr film.

#### Discussion on interface formation

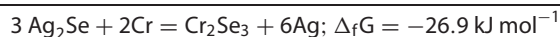
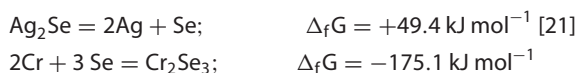
Results of GXR, AFM, XPS, and RBS studies presented in the earlier sections have shown that the thermally grown Cr film is partially oxidized and in addition there is a thin native oxide formed on

the substrate. The important outcome, however, is the inhibition of agglomeration of silver selenide film without any change in its composition or phase. The two interfaces that are crucial to the observed structural integrity of silver selenide film are those at which the partially oxidized Cr film is in contact with (i) silver selenide film and (ii) the native oxide formed on silicon.

A number of studies are available on the adhesion of Cr to oxide surfaces in general and the reaction mechanisms are well studied. Cr adheres well to oxide surfaces by forming chromium oxide during the initial stages, resulting in an oxide-oxide bond that is much stronger than that between two dissimilar surfaces (metal-oxide). For instance, a recent study<sup>[22]</sup> of Cr/alumina structure has shown that insufficient amount of chromium oxide at the interface can lead to dewetting. Adhesion of Cr can be greatly improved if the film deposition chamber is backfilled with oxygen during Cr growth.<sup>[22]</sup> In fact, most of the adhesion promoters can easily form oxides and the poor adhesion of noble metals to oxide surfaces is principally due to their poor affinity for oxygen.

Thus, in the present study, the adhesion of Cr to the native oxide-covered Si substrate may be attributed to the partial oxidation of Cr at this interface. The oxidation of Cr film during the initial stages of growth can occur either by reduction of the native silicon oxide or by gettering of the residual oxygen present in the deposition chamber by chromium. The former possibility may be ruled out, since the relevant redox reaction has a positive free energy of formation (38.4 kJ mol<sup>-1</sup>) and hence is not thermodynamically favorable.<sup>[23]</sup> In fact, Cr is shown to be un-reactive with SiO<sub>2</sub> even at 800 °C.<sup>[24]</sup> Therefore, the latter mechanism, viz. gettering of oxygen by Cr can be responsible for the Cr adhesion to the Si substrates through oxide-oxide bonding. Oxidation of Cr is possible because in the present investigations, Cr was thermally evaporated with a low rate of evaporation (~0.1 Ås<sup>-1</sup>) in relatively poor vacuum (~2 × 10<sup>-6</sup> mbar).

The role of the second interface, where silver selenide is in contact with Cr film, is equally important in promoting the adhesion of the silver selenide film. In the present case, silver selenide is formed by first depositing Se film followed by the deposition of Ag film of suitable thickness. However, Cr can react with Se to form selenides under optimal conditions. A recent study<sup>[25]</sup> of multilayer stacks of Cr and Se showed that the layers react to form Cr<sub>3</sub>Se<sub>4</sub> at 500 °C. Therefore, the reaction between Cr and Se in our samples is not expected at room temperature. However, the feasibility of the reduction reaction of Ag<sub>2</sub>Se by Cr at room temperature is examined. The redox reaction can occur through the following reaction steps.



The Gibbs free energy of formation for Cr<sub>2</sub>Se<sub>3</sub> is given as

$$\Delta_f G(\text{Cr}_2\text{Se}_3) = \Delta_f H(\text{Cr}_2\text{Se}_3) - 298.15 [S^0(\text{Cr}_2\text{Se}_3) - \{2 S^0(\text{Cr}) + 3 S^0(\text{Se})\}] = -175.1 \text{ kJ mol}^{-1}.$$

The values for different quantities used are:  $\Delta_f H(\text{Cr}_2\text{Se}_3) = -174.9 \text{ kJ mol}^{-1}$ ,<sup>[26]</sup>  $S^0(\text{Cr}_2\text{Se}_3) = 175.4 \text{ JK}^{-1} \text{ mol}^{-1}$ ,<sup>[27]</sup>  $S^0(\text{Cr}) = 23.8 \text{ JK}^{-1} \text{ mol}^{-1}$ , and  $S^0(\text{Se}) = 42.4 \text{ JK}^{-1} \text{ mol}^{-1}$ .<sup>[28]</sup>

The negative free energy of the redox reaction indicates that the reduction of Ag<sub>2</sub>Se by Cr is thermodynamically favorable even

at room temperature. However, the atmospheric exposure and the Ar-cleaning of Cr/Si during the preparation of the samples would have resulted in a thin partially oxidized layer that would serve as a barrier for the reaction of Cr with either Se or Ag<sub>2</sub>Se. In order to examine if the order of growth of Se/Ag films influence the thermal stability, studies (not presented here) were also made on silver selenide films prepared by first depositing Ag followed by Se films. These films also exhibited strong adhesion indicating that the adhesion of silver selenide films is independent of the elemental film deposited first.

Agglomeration in thin films is a thermally activated process in which the total energy of the film is minimized by continuous dewetting and gradual exposure of the substrate.<sup>[29]</sup> Recently, we have observed that silver selenide films formed directly on Si from the reaction of sequentially deposited Ag and Se films have poor adhesion and agglomerate at high temperatures.<sup>[9,10]</sup> The dewetting and consequent agglomeration is attributed to a stress-mediated two-stage process: first a large compressive stress-driven loss of film adhesion and second, grain boundary grooving mediated by interfacial energies in conjunction with thermal stress. The compressive stress builds up due to the phase change that occurs during the film formation, viz. the conversion of an initially amorphous phase (Se) into a polycrystalline phase (silver selenide) having different composition and a much larger (more than 50%) volume. The thermal stress arises during annealing, as silver selenide undergoes polymorphic phase transition at about 140 °C<sup>[30]</sup> from orthorhombic to a cubic phase with reduced volume.

The observed stability of silver selenide films in the present case shows that the presence of partially oxidized Cr film helps release the intrinsic compressive stress which otherwise can weaken film adhesion. Relief of large interfacial stresses can take place in different ways.<sup>[31]</sup> For instance, pseudomorphic growth<sup>[32]</sup> of Ge on Si, with the lattice constant of Si leads to strong compressive stress. The film relieves strain by forming a rough surface on a nanometer scale which allows partial elastic relaxation toward the Ge bulk lattice constant. Atomic rearrangement through grain boundary diffusion can also aid strain relaxation. A typical example is the stress-driven Sn whisker growth,<sup>[33]</sup> an unwanted stress relief phenomena faced in Pb-free solder technology, where the reaction of Sn and Cu generates large compressive stress. Strain relief can also take place through morphological instabilities at the interface, like island formation.<sup>[34]</sup> A film may delaminate<sup>[35]</sup> from the substrate if the compressive stresses are much stronger than the adhesive forces between the film and the substrate.

We believe, in the present case, the most likely mechanism that is operative in the compressive stress relief is the growth of grains<sup>[32,36,37]</sup>, which maximizes the resulting surface area. Compressive stress relief through grain growth has been observed in different systems and is attributed to the reduction of strain energy at the cost of a large increase in film-surface area.<sup>[32]</sup> This explanation based on the surface morphology of the as-deposited films will become clear if we compare the morphologies of silver selenide films grown on Si substrates with and without Cr film. Shown in Fig. 9 are the AFM images of the as-deposited and 100 °C annealed films that were grown on Cr/Si together with the corresponding images of those deposited directly on Si. All the images have the same area of 2.5 μm × 5 μm. A clear difference in the morphologies of the as-deposited film grown on Cr/Si (Fig. 9(a)) and the film grown directly on Si (Fig. 9(b)) can be seen. The growth of grain clusters (Fig. 9(a)) consisting of smaller grains rather than the formation of large grains at the expense of smaller

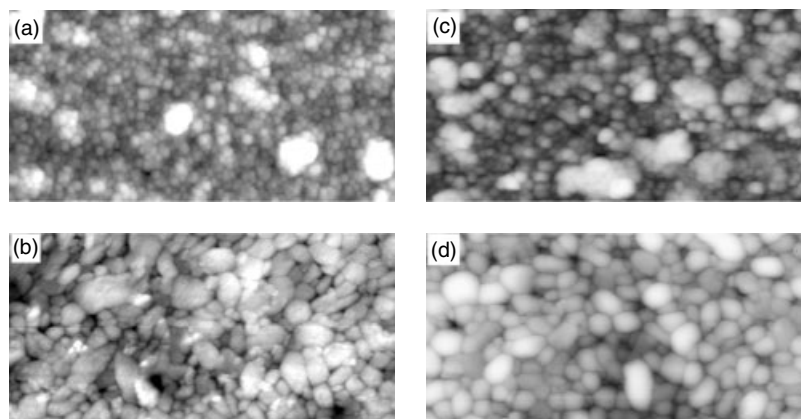


**Figure 9.** AFM images ( $2.5 \mu\text{m} \times 5 \mu\text{m}$  scanned area) of as-deposited films grown on (a) Cr/Si and (b) bare Si substrates. The corresponding images of the films annealed at  $100^\circ\text{C}$  are shown in (c) and (d) respectively.

grains reflects the tendency of the film to maximize the surface area, which helps in compressive stress relief. The film grown on Si on the other hand, shows (Fig. 9(b)) grains with random shape exhibiting poor adhesion.<sup>[9,10]</sup> The fact that both the films are not under significant compressive stresses is confirmed by XRD measurements, as the calculated lattice spacings are found to be close to the ASTM standards.

Further evidence for the specific strain relief route followed by each film can be obtained from the evolution of their surface morphology upon annealing at  $100^\circ\text{C}$ . Figures 9(c) and 9(d) present AFM images of the film grown on Cr/Si and the film grown directly on Si. Both films are annealed at  $100^\circ\text{C}$  for 60 min under flowing Ar. The film on Cr/Si does not show significant change in grain shape (Fig. 9(c)). On the other hand, the film on Si which has poor adhesion<sup>[9,10]</sup> exhibits large increase in grain size (Fig. 9(d)). Such large increase in the average grain size can cause the buildup of tensile stress<sup>[38]</sup> and eventual film agglomeration.

Thus, the films deposited on Cr/Si as well as those grown on Si without any intermediate film release elastic energies, although through different ways: the former by the development of a specific morphology, while the latter by losing its adhesion to the substrate. This difference in growth modes may be attributed to the underlying partially oxidized Cr film, since the method adopted for the growth of silver selenide film is the same for both the cases. In order to understand the importance of the partially oxidized Cr film in aiding the growth of the observed morphology, we formed silver selenide films under similar conditions on commonly used substrates such as glass, fused quartz, and Si having intentionally grown native oxide, and examined their thermal stability. The results (not presented here) showed that all the films were unstable and agglomerated into well-separated islands with anneal temperature increasing to  $400^\circ\text{C}$ . This clearly demonstrates that Cr film, although partially oxidized, is crucial to the formation of the morphology that accounts for stress relief.

The formation of grain clusters instead of large grains may be explained on the basis of the preferential growth of silver selenide on nucleation centers. Thermally evaporated Cr films at  $\sim 10^{-6}$  mbar are known to contain various defects. Further, the nature and number density of these defects will be changed if the films are exposed to air. When there is a distribution of defects, growth of nucleating species is promoted on defects having a low energy barrier to the formation of nuclei.<sup>[39,40]</sup> We believe that the majority of defects in the partially oxidized Cr film have a low energy barrier to the formation of silver selenide nuclei. Therefore, preferential

growth of silver selenide occurs on these sites, which eventually leads to the development of grain clusters. In fact, vapor-deposited metal films on substrates with partially oxidized thin metal films have been studied in detail.<sup>[41]</sup> The results have clearly indicated the formation of grain clusters rather than coalescence of small grains into large grains.

## Summary

In summary, we have investigated in detail the thermal stability of silver selenide films formed on thin Cr film coated with Si from the solid-state reaction of sequentially deposited Ag and Se. The phase, surface morphology, and structural integrity of the films have been probed using GXR, XPS, AFM, and RBS. The results show that the films remain stable without any phase or compositional change when annealed up to a maximum temperature of  $400^\circ\text{C}$ , used in the studies. A possible explanation for the improved stability of silver selenide films is offered based on the compressive stress relief by a surface morphology consisting of large number of grains with an overall high surface area. The formation of this specific morphology that maximizes surface area has been attributed to the nucleated growth of silver selenide films on the partially oxidized Cr adhesion film.

## Acknowledgement

The authors thank Mr S. C. Choudhury, IOP, Bhubaneswar for his help in carrying out the XPS measurements. One of the authors (BCM) thanks the Council of Scientific and Industrial Research, India for providing a financial support in the form of a Senior Research Fellowship.

## References

- [1] S. W. Russell, S. A. Rafalski, R. L. Spreitzer, J. Li, M. Moinpour, F. Moghadam, T. L. Alford, *Thin Solid Films* **1995**, *262*, 154.
- [2] Y. Tsuji, S. M. Gasser, E. Kolawa, M.-A. Nicolet, *Thin Solid Films* **1999**, *350*, 1.
- [3] C.-Y. Yang, J. S. Chen, *J. Electrochem. Soc.* **2003**, *150*, G826.
- [4] Y. Zeng, Y. L. Zou, T. L. Alford, F. Deng, S. S. Lau, T. Laursen, B. Manfred Ullrich, *J. Appl. Phys.* **1997**, *81*, 7773.
- [5] W. M. Liao, Y. P. Lin, F. T. Yuan, S. K. Chen, *J. Magn. Magn. Mater.* **2004**, *272–276*, 2175.

- [6] C.-C. Leu, H.-T. Lin, C.-T. Hu, C.-H. Chien, M.-J. Yang, M.-C. Yang, T.-Y. Huang, *J. Appl. Phys.* **2002**, *92*, 1511.
- [7] G. Safran, O. Geszti, G. Radnoczi, P. B. Barna, *Thin Solid Films* **1998**, *317*, 72.
- [8] J. Janek, B. Mogwitz, G. Beck, M. Kreuzbruck, L. Kienle, C. Korte, *Prog. Solid State Chem.* **2004**, *32*, 179.
- [9] B. C. Mohanty, B. S. Murty, V. Vijayan, S. Kasiviswanathan, *Appl. Surf. Sci.* **2006**, *252*, 7975.
- [10] B. C. Mohanty, S. Kasiviswanathan, *Thin Solid Films* **2006**, *515*, 2059.
- [11] M. Hansen, *Constitution of Binary Alloys*, McGraw-Hill: New York, **1958**, p 49.
- [12] M. Mayer, *Nucl. Instrum. Methods B* **2002**, *194*, 177.
- [13] International Centre for Diffraction Data, *JCPDS Powder Diffraction Database*, PDF-2, **1997**, pp 24.
- [14] B. C. Mohanty, A. K. Tyagi, A. K. Balamurugan, S. Varma, S. Kasiviswanathan, *Nucl. Instrum. Methods B* **2008**, *266*, 1480.
- [15] International Centre for Diffraction Data, *JCPDS Powder Diffraction Database*, PDF-2, **1997**, pp 44.
- [16] R. Kwok, *XPSPEAK 4.1*, **2000**, <http://www.phy.cuhk.edu.hk/~surface/XPSPEAK/>.
- [17] M. Romand, M. Roubin, J. P. Deloume, *J. Electron Spectrosc. Relat. Phenom.* **1978**, *13*, 229.
- [18] D. Briggs, J. C. Riviere, Spectral interpretation, in *Practical Surface Analysis, Auger and X-ray Photoelectron Spectroscopy* (Eds: D. Briggs, M. P. Seah), John Wiley & Sons: New York, **1983**, p 128.
- [19] R. Chen, D. Xu, G. Guo, Y. Tang, *J. Mater. Chem.* **2002**, *12*, 1437.
- [20] M. Shenasa, S. Sainkar, D. Lichtman, *J. Electron Spectrosc. Relat. Phenom.* **1986**, *40*, 329.
- [21] F. Gronvold, S. Stolen, Y. Semenov, *Thermochim. Acta* **2003**, *399*, 213.
- [22] R. W. Pierce Jr, J. G. Vaughan, *IEEE Trans. Compon., Hybrids, Manuf. Technol.* **1983**, *6*, 202.
- [23] P. T. Vianco, C. H. Sifford, J. A. Romero, *IEEE Trans. Ultrason. Ferroelectr. Freq. Control* **1997**, *44*, 237.
- [24] R. Pretorius, J. M. Harris, M.-A. Nicolet, *Solid State Electron.* **1978**, *21*, 667.
- [25] M. Behrens, R. Kiebach, W. Bensch, *Inorg. Chem.* **2006**, *45*, 2704.
- [26] Yu. D. Tretyakov, I. V. Gordeev, Ya. A. Kesler, *J. Solid State Chem.* **1977**, *20*, 345.
- [27] A. V. Blinder, A. S. Bolgar, Zh. A. Trofimova, *Powder Metall. Met. Ceram.* **1993**, *32*, 234.
- [28] R. C. Weast, M. J. Astle, *CRC Handbook of Chemistry and Physics* (61st edn), CRC Press: Boca Raton, **1980**, pp D62.
- [29] J.-Y. Kwon, T.-S. Yoon, K.-B. Kim, S.-H. Min, *J. Appl. Phys.* **2003**, *93*, 3270.
- [30] N. G. Dhere, A. Goswami, *Thin Solid Films* **1970**, *5*, 137.
- [31] L. B. Freund, S. Suresh, *Thin Film Materials: Stress, Defect Formation and Surface Evolution*, University Press: Cambridge, **2003**.
- [32] P. Zahl, P. Kury, M. Horn von Hoegen, *Appl. Phys. A* **1999**, *69*, 481.
- [33] K. N. Tu, J. O. Suh, A. T. Wu, in *Lead-free Solder Interconnect Reliability* (Ed.: D. Shangguan), ASM International: Materials Park, **2005**, p 147.
- [34] J. Müller, M. Grant, *Phys. Rev. Lett.* **1999**, *82*, 1736.
- [35] H. Windischmann, *Crit. Rev. Solid State Mater. Sci.* **1992**, *17*, 547.
- [36] P. Chaudhari, *J. Vac. Sci. Technol.* **1972**, *9*, 520.
- [37] C. V. Thompson, R. Carel, *J. Mech. Phys. Solids* **1996**, *44*, 657.
- [38] C. van Opdorp, M. Verkerk, *J. Appl. Phys.* **1988**, *63*, 1518.
- [39] Z. Kozisek, M. Hikosaka, P. Demo, A. M. Sveshnikov, *J. Cryst. Growth* **2005**, *275*, e79.
- [40] F. Nouvertne, U. May, A. Rampe, M. Gruyters, U. Korte, R. Berndt, G. Guntherodt, R. Pentcheva, M. Scheffler, *Phys. Rev. B* **1999**, *60*, 14382.
- [41] S.-I. Kobayashi, *Surf. Sci. Rep.* **1992**, *16*, 1.